Observation of electric polarization reversal and magnetodielectric effect in orthochromites: A comparison between $LuCrO_3$ and $ErCrO_3$

K. R. S. Preethi Meher,[1,2] Alexandre Wahl,[1,2] Antoine Maignan,[1,*] Christine Martin,[1] and Oleg I. Lebedev[1]
[1]*Laboratoire CRISMAT, UMR 6508 CNRS/ENSICAEN/UCBN, 6 Boulevard Marechal Juin, 14050 Caen cedex, France*
[2]*CNRT 6 Boulevard Marechal Juin, 14050 Caen cedex, France*
(Received 30 September 2013; revised manuscript received 3 February 2014; published 1 April 2014)

The presence of electric field–induced polarization reversal behavior just below Néel's antiferromagnetic ordering temperature (T_N) is demonstrated in polycrystalline orthorhombic $LuCrO_3$, which crystallizes in the centrosymmetric space group (*Pbnm*) at room temperature. This result on $LuCrO_3$ is compared with $ErCrO_3$, another orthochromite. The single phase nature and the quality of both polycrystalline samples were checked by x-ray diffraction and transmission electron microscopy (TEM). The high-resolution TEM images of $LuCrO_3$ and $ErCrO_3$ brought out the presence of twin boundaries. Detailed magnetic, dielectric, and polarization studies were carried out on both systems. As the presence of ferroelectric-like characteristics is found below T_N in both $LuCrO_3$ and $ErCrO_3$, this rules out the condition for the rare earth cation to be paramagnetic for observing possible signatures of multiferroicity in this family of compounds. Also, we report a much stronger magnetodielectric effect in the case of $ErCrO_3$ compared with $LuCrO_3$ reflecting the different magnetism of their *A*-site cations.

DOI: 10.1103/PhysRevB.89.144401 PACS number(s): 75.85.+t, 75.47.Lx, 68.37.Og, 77.22.Ej

I. INTRODUCTION

Rare earth orthochromites of $RCrO_3$ composition, where R is a lanthanide ion, have been under study for several decades in pursuit of their interesting magnetic properties [1–12]. More recently, the studies by Rajeswaran *et al*. [13] shed light on this family of antiferromagnets, as they reported evidence of multiferroicity. These authors showed that some orthochromite ($RCrO_3$) ceramics could be ferroelectric below their antiferromagnetic ordering temperature T_N only for the paramagnetic R^{3+} cation. This was established by observation of polarization below T_N along with reversal of this polarization subsequent to poling with positive and negative electric fields. Whatever the magnetic nature of the R^{3+} cation is, the structure of most orthochromites remains centrosymmetric, and the magnetic structures do not lead to a magnetic point group that breaks the space inversion symmetry below the chromium sublattice magnetic ordering temperature. Only in the case of $TbCrO_3$, $DyCrO_3$, and $GdCrO_3$ can one find a magnetic symmetry group that supports polarization below the rare earth magnetic ordering temperature [14,15]. This motivated us to revisit two polycrystalline members of the orthochromites with a diamagnetic ($R = Lu^{3+}$) and a paramagnetic ($R = Er^{3+}$) cation.

In the present investigation, we reveal the presence of a possible ferroelectric state in both $LuCrO_3$ and $ErCrO_3$ polycrystalline samples below T_N, as evidenced by net polarization, that is clearly absent for temperatures above T_N. For both systems, this net polarization reverses under sign change of the applied electric field used for poling. Our results, showing that the paramagnetic nature of the *A* cation is not necessary to observe the multiferroic-like characteristics in orthochromites, calls for structural and magnetic studies to explain the origin of these features.

*Corresponding author: antoine.maignan@ensicaen.fr

II. EXPERIMENTAL

The polycrystalline samples were prepared by solid state reaction in air at 1400 °C: stoichiometric proportions of Er_2O_3 (Lu_2O_3) and Cr_2O_3 powders were crushed before pressing into bars ($2 \times 2 \times 10$ mm) prior to sintering in air. The quality of the samples was checked by x-ray diffraction (XRD) and transmission electron microscopy (TEM; Tecnai G2 30 UT microscope operated at 300 kV and having 0.17-nm point resolution). The TEM sample was prepared by dispersing the crushed powders in methanol and spreading it out on a Cu carbon holey grid. Energy-dispersive x-ray spectroscopy performed by an EDAX system with the same TEM (10–15 crystallites analyzed, 60-s acquisition time) confirm cation contents very close to the nominal ones. Aberration-corrected high-resolution TEM (HRTEM), annular dark field scanning TEM (STEM) were carried out on a JEM ARM 200 F double-corrected microscope equipped with a Centurio EDS spectrometer. All experiments were carried out at 200 kV acceleration voltage. Pieces of bar samples were used for magnetization measurements with a superconducting quantum interference device magnetometer (Quantum Design Inc.). The sintered rectangular bars were cut into smaller slabs of around 1 mm thick for dielectric and polarization measurements. Silver electrodes were painted on the parallel faces of the sintered samples and dried at room temperature. Subsequently, thin Cu leads were attached to the electrode faces with the same silver paint. Capacitance and dissipation factor of these samples were measured as a function of temperature and frequency with a Agilent 4284A LCR meter. The dielectric constant (ε_r') and loss ($\tan\delta$) were measured as a function of temperature in the range of 8 to 180 K at a heating rate of 2 K/min. Polarization measurements were carried out with the aid of an electrometer (Keithley 6200 model). The sample was heated/cooled in a PPMS 14 T (Quantum Design) during measurement. Before carrying out polarization measurements, the $LuCrO_3$ (LCO) sample was poled by applying an electric field of 165 kV/m at 140 K ($T > T_N$) and subsequently cooled

down to 8 K. The $ErCrO_3$ (ECO) sample was poled at 160 K in a similar range of applied electric field values before cooling across T_N. Measurements commenced only after nulling the current drift by waiting 1–2 hours after poling. Charge across the sample was measured as a function of temperature from 8 to 200 K at a heating rate of 5 K/min.

III. RESULTS

The XRD patterns show that the samples are single phased, and the structures have been refined in *Pbnm*, with $a = 5.2269(1)$ Å, $b = 5.5126(1)$ Å, $c = 7.5212(2)$ Å ($V = 216.716(6)$ Å^3) for ECO and $a = 5.1773(1)$ Å, $b = 5.4964(1)$ Å, $c = 7.4774(2)$ Å ($V = 212.783(5)$ Å^3) for LCO, in agreement with the literature [1]. The structure is also confirmed by ED: the spots obey the reflection conditions imposed by the *Pbnm* space group. As expected, the ED patterns are similar for ECO and LCO. The latter are shown in Figs. 1(a)–1(d). The presence of *h00, 0k0,* and *00l* with $h, k, l = 2n + 1$ spots are explained by double diffraction. A HRTEM study has been performed for both compounds, leading to similar results; consequently, only the LCO results are presented. The uniform contrast of HRTEM images [Figs. 2(a)–2(c)] shows the high quality of the crystalline structure: no sign of defects, stacking faults, or cation/anion vacancies are observed. However, owing to the orthorhombic symmetry, twinning phenomena occur, as usually reported in perovskites [16,17]. In the bright-field (BF) HRTEM image viewed along the [110] direction [Fig. 3(a)] two orientated domains are evidenced. The *c* axis is oriented at 90° from one region to the other (c_1 and c_2) creating a sharp twin boundary along the ⟨112⟩ twin plane, as schematized in Fig. 3(b). Another type of twinning is observed in the [001] HRTEM image [Fig. 3(c)], implying a permutation of the *a* and *b* axes that induces a spot splitting of higher order reflections in the ED pattern [marked by white arrows in the inset of Fig. 3(c)]. The annular bright field (ABF)-STEM image of

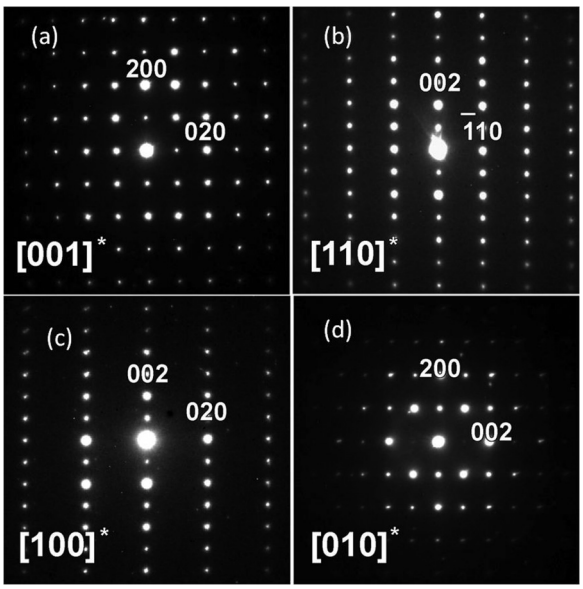

FIG. 1. ED patterns of LCO along four main zone axis: (a) $[001]^*$, (b) $[110]^*$, (c) $[100]^*$, (d) $[010]^*$.

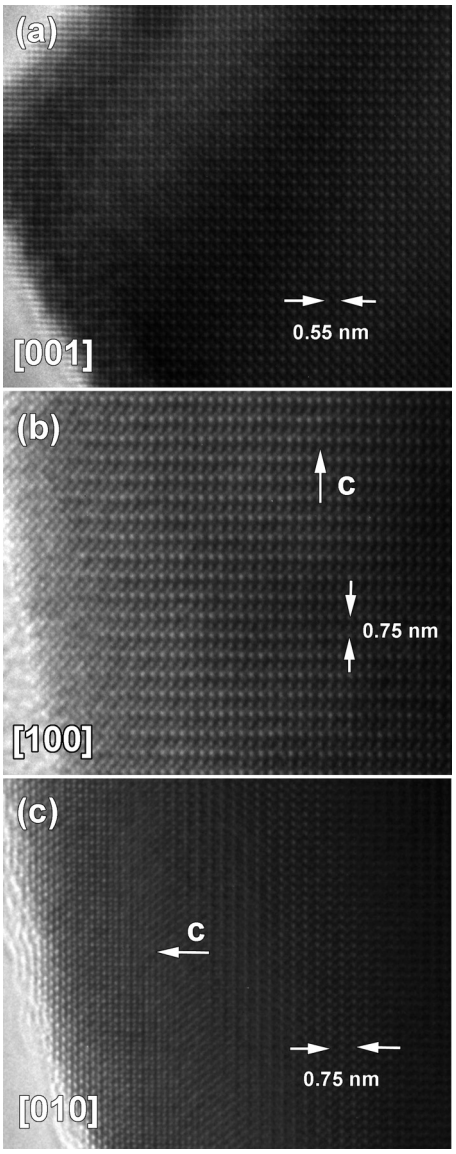

FIG. 2. Bright-field HRTEM images of LCO along: (a) [001], (b) [100], (c) [010].

the twin boundary [Fig. 3(d)] is consistent with the structural model drawn in Fig. 3(e). The twin plane is (220) [Fig. 3(c)], which is consistent with the unsplit *hh0* row of spots in the ED pattern. The presence of these extended twinning planes could affect the physical properties.

To check the consistency of magnetic behavior with existing data, temperature dependence of magnetization was collected [Figs. 4(a) and 4(b)]. For LCO, only one transition is observed around 116 K, in good accordance with that reported in earlier literature [2,7]. As Lu^{3+} is not a magnetically active ion, the magnetic characteristics are entirely attributed to the magnetic ordering of the $S = 3/2$ Cr^{3+} cations in the case of LCO. For ECO, two magnetic transitions are observed at $T_N \sim 133$ K and $T_{SR} \sim 22$ K, where T_{SR} is the spin reorientation temperature, as reported in the literature, which results from coupling between the chromium and erbium magnetic moments [1–5].

Before subjecting the LCO and ECO ceramics to dielectric measurements, it is very important to verify their leakage

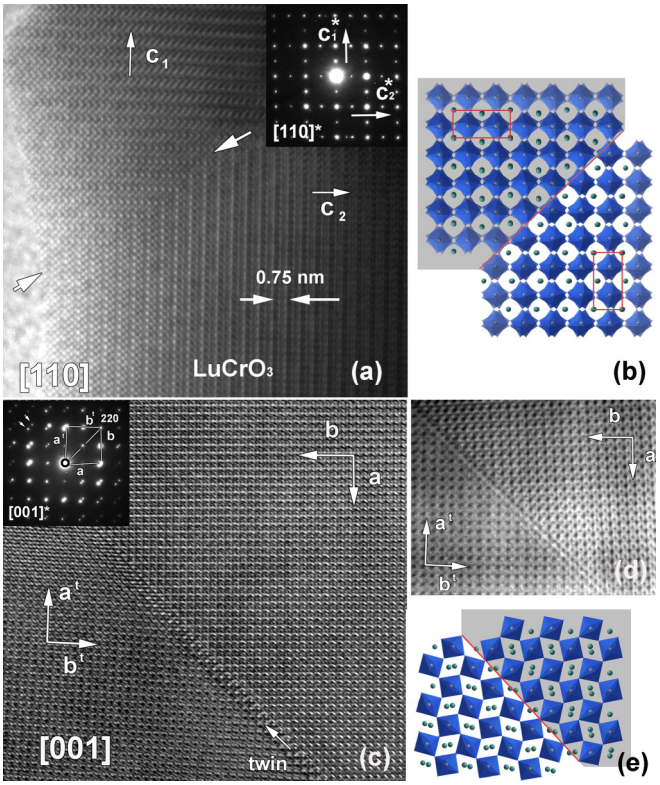

FIG. 3. (Color online) (a) Bright-field [110] HRTEM image of 90° rotational twinning in LCO. The inset shows corresponding ED patterns, which are superpositions of two $[110]^*$ ED patterns from different domains rotated 90° with respect to each other. Corresponding structural model is presented in (b) (Lu = dark green spheres, CrO_6 octahedras are in blue). Twin plane is depicted by red line. (c) Aberration-corrected bright-field [001] HRTEM image of permutation twin in LCO and corresponding ED pattern given as insert in upper left corner. Note the splitting of higher order spots marked by white arrows due to the twinning; (d) annular dark field STEM image of the same twin boundary shown in panels (c) and corresponding structural model (Lu = dark green spheres, CrO_6 octahedras are in blue) (e). Twin plane is depicted by red line.

characteristics. Figures 5(a)–5(f) shows the dielectric constant (ε_r'), loss factor (tanδ), and AC conductivity (calculated from the relation $\sigma_{AC} = 2\pi f \varepsilon_r' \varepsilon_0 \tan\delta$) as a function of frequency (f) for LCO (left-hand side) and ECO (right-hand side) at various temperatures. The absence of dispersion in both ε_r' and tanδ values over the entire frequency range for $T \leqslant 100$ K shows the lack of space charge or charge-hopping mechanisms. AC conductivity values remain almost constant and very low ($\sim 10^{-10}$ S/m) up to 100 K for LCO but increase notably above 100 K due to an increase in overall conductivity. A similar trend is observed in the case of ECO, except that the σ_{AC} values are an order lower than that of LCO in the measured frequency and temperature ranges. As the conductivity increases significantly with temperature [see $T = 150$ K and 200 K in Figs. 5(c) and 5(d)], space charge starts to build up at lower frequencies. This is more evident by the steplike relaxation at low frequencies (<10 kHz) in AC conductivity [Figs. 5(e)] accompanied by a broad peak in the tanδ curve at 200 K for LCO [see Fig. 5(c)]. This feature is just imminent in the case of ECO at 200 K due to its comparatively resistive nature [see Figs. 5(d) and 5(f)]. Therefore, the influence of ionic/electronic conductivity on the dielectric measurements can be neglected at temperatures up to 150 K at higher frequencies for ECO. This is not the case for LCO, where the conductivity characteristics start to dominate the dielectric measurements just above 100 K, even at higher frequencies.

Dielectric permittivity (ε_r') of LCO was measured as a function of temperature down to 8 K at four selected frequencies between 5 and 500 kHz, and for sake of clarity, only the 500-kHz curve is shown in Fig. 4(c). $\varepsilon_r'(T)$ and tan$\delta(T)$ do not exhibit a noticeable anomaly around T_N (~116 K), which might be explained by the significant increase in electrical conductivity above 100 K, as attested by the tan$\delta(f)$ curve collected at 150 K in Fig. 5(c). In contrast, for ECO, two distinct peaks occur at T_N (~133 K) and T_{SR} (~22 K) in $\varepsilon_r'(T)$ [Fig. 4(d)] pointing toward the existence of magnetodielectric coupling. The conductivity values lower than those of LCO might explain why ε_r' changes at T_N for ECO.

The curves of the relative polarization ΔP ($\mu C/m^2$) as a function of temperature are given in [Figs. 4(e) and 4(f)]. For LCO, the largest ΔP is in the range of ~90 $\mu C/m^2$ at the lowest temperature of measurement. The transition in ΔP behavior is not sharp; rather, it proceeds in two stages, with a first transition at $T_N \sim 116$ K [Figs. 4(a) and 4(e)] and a more diffuse transition extending up to ~160 K. This ΔP can be reversed by reversing the polarity of the poling electric field [Fig. 4(e)]. For ECO, the measured polarization values notably drop down around T_N, supporting a possible transition from polar antiferromagnetic state to a nonpolar paramagnetic state [Fig. 4(f)]. The maximum ΔP values obtained are in the range of ~70 $\mu C/m^2$ (below T_N). This polarization could also be reversed by reversing the polarity of the applied electric field. To confirm the ferroelectric nature below T_N, ΔP values have also been measured as a function of temperature at different poling electric fields (E) encompassing the 17–175 kV/m range. When ΔP values are plotted as a function of applied electric field [inset of Fig. 4(f)], at 8 K it roughly mimics the first quadrant of a typical $P(E)$ hysteresis loop, and the upturn in $\Delta P(E)$ behavior indicates an alignment of most of the dipoles above ~60 kV/m. The characteristic value of the electric field at the change of slope in $\Delta P(E)$ behavior also weakens with the decrease of ΔP as T approaches T_N. Compared with ECO, the ΔP *vs* T behavior of LCO exhibits a more diffuse transition around T_N that can be attributed to the more leaky nature of LCO. A significant increase in thermally stimulated current could make the transition appear more diffusive. Despite these dominating effects in LCO, the above results suggest the existence of a polar state induced by magnetic ordering below T_N. However, polarization could not be significantly modified by applying a magnetic field (up to 9 T) below T_N for both ECO and LCO, so that the magnetoelectric coupling is not evidenced.

In order to probe the existence of magnetodielectric coupling, dielectric measurements were performed with an applied magnetic field up to ±5 T on LCO and ECO at different temperatures from below and above T_N [Figs. 6(a) and 6(b), respectively]. For LCO, at 8 K, ε_r' decreases with increase in H, and significant hysteresis is observed when the magnetic field is swept back. The magnetodielectric (MD)

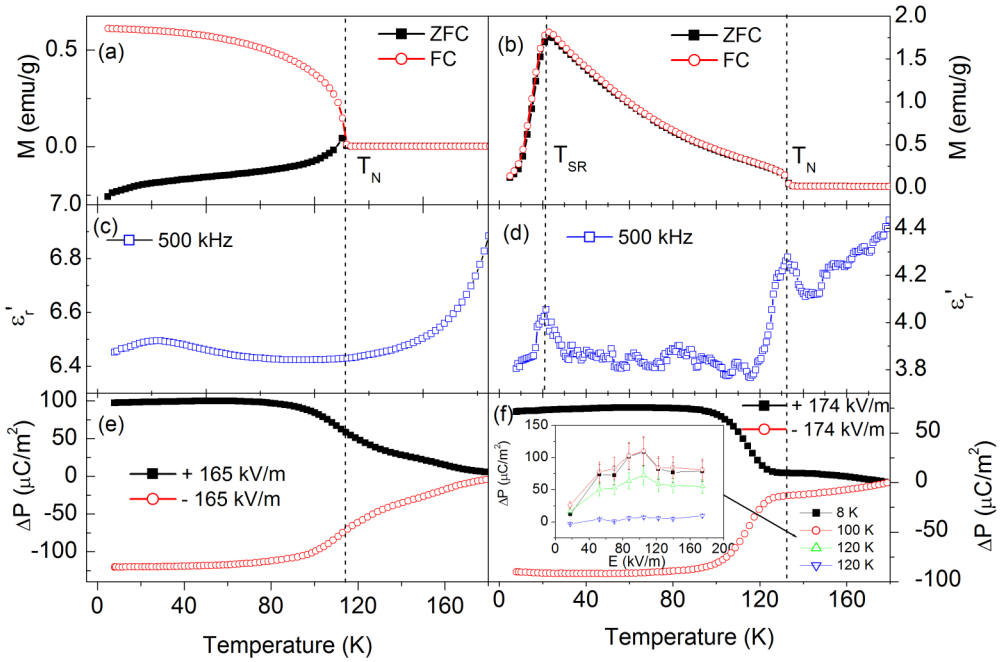

FIG. 4. (Color online) (a) Magnetization as a function of temperature under zero field–cooled (ZFC) and field-cooled (FC) conditions at 100 Oe for LCO. (b) Magnetization as a function of temperature measured under both ZFC and FC conditions at 100 Oe for ECO. Dielectric constant (ε_r') as a function of temperature recorded at an applied frequency of 500 kHz for (c) LCO and (d) ECO. (e) ΔP as a function of temperature recorded at 5 K/min for LCO and applied electric field of 165 kV/cm in both positive and negative polarity for LCO. (f) The net change in polarization (ΔP) measured as a function of temperature at a heating rate of 5 K/min for ECO and applied electric field of 174 kV/m in both positive and negative polarity. The inset of this figure shows ΔP as a function of applied electric field at different temperatures encompassing T_N.

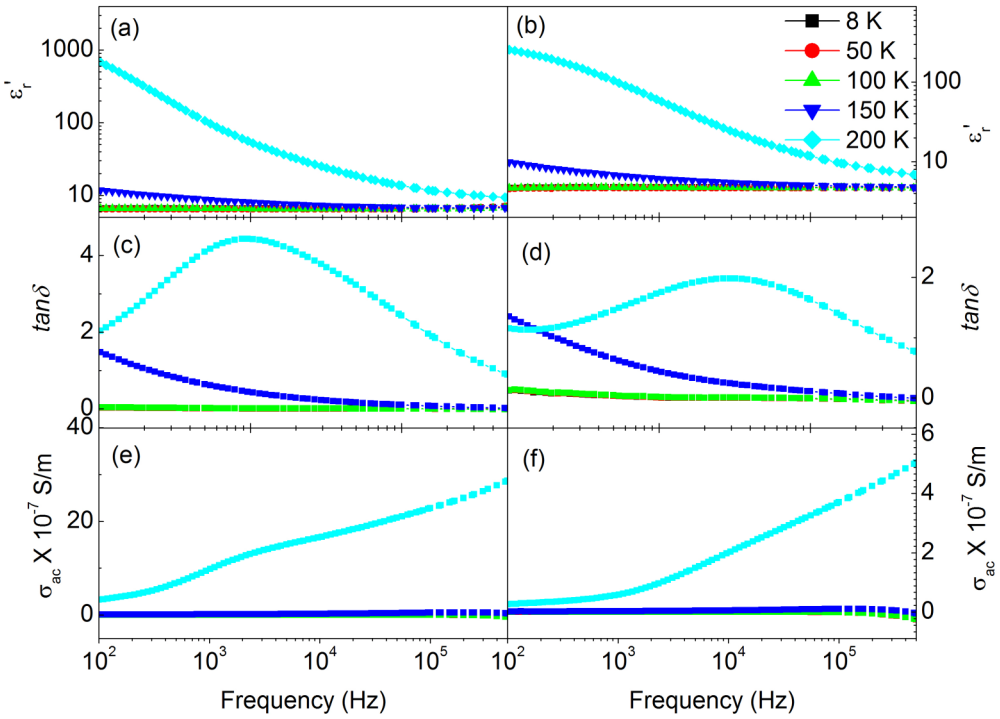

FIG. 5. (Color online) (a)–(f) Dielectric constant (ε_r), loss factor (tanδ), and AC conductivity (σ_{AC}) of LCO (on right-hand side) and ECO (left-hand side) as a function of frequency (1–500 kHz) at different temperatures, such as 8, 50, 100, 150, and 200 K, respectively.

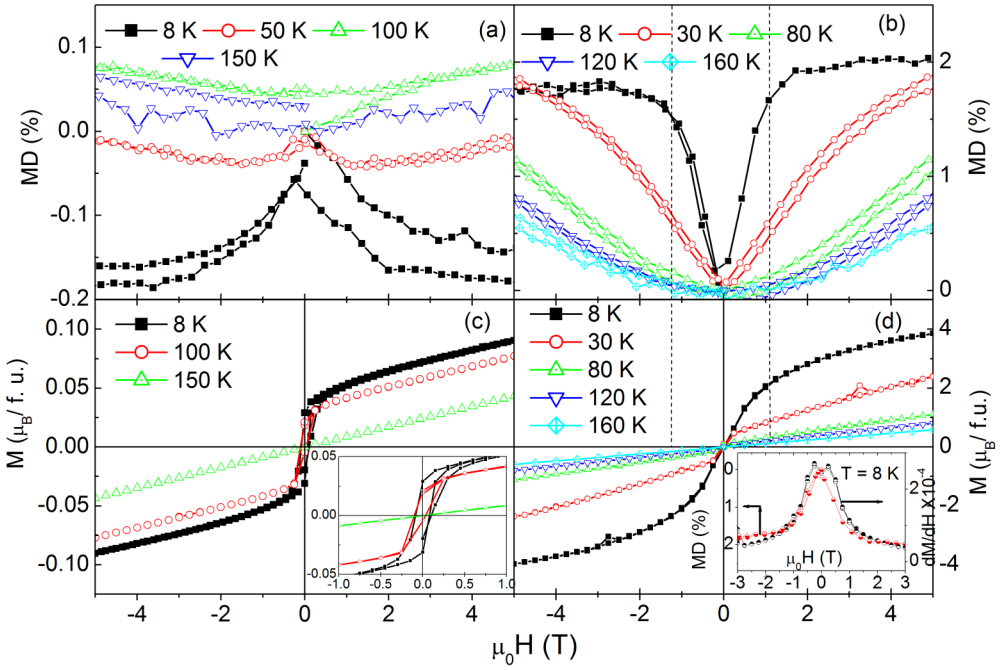

FIG. 6. (Color online) MD effect (%) obtained by sweeping the applied magnetic field (H) at a rate of 50 Oe/s at different temperatures and applied frequency of 100 kHz for (a) LCO and (b) ECO. Magnetization as a function of applied magnetic field (H) recorded at different temperatures for (c) LCO and (d) ECO. The dM/dH curve and MD (%) obtained at 8 K for ECO as a function of magnetic field is shown in the inset of Fig. 6(d).

effect (%) of LCO [Fig. 6(a)] is calculated for $f = 100$ kHz by using the equation MD $= \{[\varepsilon_r'(H) - \varepsilon_r'(H = 0)]/\varepsilon_r'(H = 0)\} \times 100$. The calculated MD effect is clearly negative with maximum |MD| values of ∼0.2% at 8 K. As T approaches T_N, the MD effect is positive and tends to be more linear at $T = 100$ K and 150 K, with net change in the values being insignificant compared with that of low temperatures. Figure 6(c) shows the magnetization *vs* H curves for LCO recorded at various temperatures such as 8 K, 100 K, and 150 K in the magnetic field range (±5 T). They indicate the presence of a weak ferromagnetic moment below T_N [enlargement shown in the inset of Fig. 6(c)]. However there is no striking correlation between the MD(H) and M(H) curves of LCO except that the change in ε_r' with H weakens with the decrease in ferromagnetic component until it disappears at T_N. At $T = 8$ K, the MD effect of ECO shown in Fig. 6(b) is positive, contrasting with the negative values obtained for LCO, and the MD of 2%, is one order of magnitude higher than that observed for LCO. Furthermore, from the $\varepsilon'(H)$ curve collected at 8 K for ECO, a superior sensitivity $d\varepsilon_r'/dH = 0.0569/T$, up to a critical magnetic field value $H_c = 1.6$ T, is observed compared with only $0.00138/T$ above $H_c = 1.6$ T and up to the maximum applied magnetic field of 5 T. For ECO, the $\varepsilon_r'(H)$ curve tends to be more linear as T goes beyond the T_{SR}, with no significant change as T approaches T_N. The larger MD effect in ECO below its spin reorientation temperature suggests that the MD effect is driven mostly by the magnetic interaction between Er^{3+} and Cr^{3+} cations [12]. The M(H) loops recorded for ECO exhibit a weak ferromagnetic component due to the canted antiferromagnetic structure in the T range $T_{SR} < T < T_N$ [$T = 30$, 80, and 120 K in Fig. 6(d)]. Below T_{SR} [$T = 5$ K in Fig. 6(d)], a typical S-shaped curve is observed as the Er^{3+} paramagnetic moment dominates at this temperature. When the magnetic field–dependent magnetic susceptibility ($\chi = dM/dH$) curve extracted from the M(H) loops of ECO is plotted along with the MD (%) curve at $T = 8$ K [shown in the inset of Fig. 6(d)], one observes a close correlation between the two trends, suggesting stronger magnetoelastic coupling effects induced by spin reorientation. This behavior resembles the magnetoelastically induced MD coupling characteristics reported in some other oxide systems, such as $HoMnO_3$ and CoV_3O_8 [18,19].

IV. DISCUSSION

Our experimental results obtained on $LuCrO_3$ suggest the existence of a possible ferroelectric state below T_N, evidenced by the observation of a net polarization change below T_N after a poling process and the reversal of this polarization by reversing the sign of the poling field. This result for LCO (i.e., for a diamagnetic A-site cation) is in marked contrast to the report by Rajeswaran *et al.* [13], although similar results are observed for $ErCrO_3$. For the latter, the anomalies observed in dielectric permittivity *vs* T and polarization *vs* E support the possibility of ferroelectricity below T_N in these orthochromites. At this point, it is worth commenting on the ferroelectric characterization of the present samples compared with conventional ferroelectrics. Though a ΔP change below T_N and its reversal with a change in sign for E are features expected in typical multiferroics, too high conductivity and/or existence of defects can lead to spurious effects on the P measurement. For a typical ceramic of conductivity 10^{-11} S/cm and remnant polarization of 0.01 μC/cm^2, the leakage current and the polarization current could be of similar magnitudes. Thus, a faster switching time

would be required to separate out the actual polarization and the leakage currents through $P(E)$ measurement at higher frequencies. In addition, because the polycrystalline samples have the tendency to accommodate defects and vacancies at their grain boundaries, the release of such charges at higher temperatures also leads to larger changes in the observed polarization values [20]. Unless measurements on single crystals are performed, spin-induced ferroelectricity cannot be claimed.

From the structure point of view, the observation of polarization reversal characteristics below T_N, irrespective of the magnetic nature of the A-site cation, is controversial. In fact, as explained in the comment on the experimental observation of polarization below T_N in $SmFeO_3$, the possibility of symmetry breaking below the Fe (or Cr) ordering temperature for the *Pbnm* space group in these systems has to be ruled out [15]. This calls for a discussion on possible origins for the results obtained on orthochromites. For instance, one cannot exclude the possible role of magnetic domain walls. Reports, especially on the low-temperature domain wall dynamics in several orthoferrites, and recent ones on systems such as iron borate and hematite, have contributed to a better understanding [21–24]. Due to their pseudocubic structure, the *Pbnm* perovskites have a tendency to possess twin boundaries. An earlier report on some of the orthoferrites suggested that the magnetic domain wall motion can be impeded significantly by the presence of twin boundaries [25]. Only in the case of $GdCrO_3$, the interactions among composite domain walls, which are ferroelastic, ferromagnetic, and therefore multiferroic in nature, have been invoked to explain the ferroelectric characteristics observed below the Gd ordering temperature [26]. Also, studies engaging resonant ultrasound spectroscopy on polycrystalline antiferromagnetic hematite support the existence of sufficient strain around the magnetic ordering temperature due to the ferroelastic nature of magnetic domain walls [27]. These recent reports have bolstered further understanding of the coupling between ferroelastic and antiferromagnetic order parameters through strain. Therefore the twin boundaries, observed at room temperature in our TEM investigations for both $ErCrO_3$ and $LuCrO_3$, could pin the magnetic domain walls when cooled just below T_N and eventually induce a symmetry breaking strain in response to the large stress field, which in this case is generated by the applied electric field during poling. Further studies employing complementary experimental techniques on both single-crystal and polycrystalline samples of orthochromites may be required to prove this hypothesis. Weak lattice distortions or lattice strains involving any Cr off-centering below T_N cannot be ruled out. Therefore, one cannot ignore the possibility for synergetic effects between the ferroelastic nature of domain walls and very weak lattice distortions involving any Cr off-centering that is too weak to break the structural symmetry but becomes noticeable due to poling. A last hypothesis based on chromium mixed valency resulting from stoichiometric deviations can be considered. Below T_N, the Cr^{3+}-Cr^{3+} superexchange interaction would localize the charge carriers (Cr^{2+} or Cr^{4+}), resulting in a better insulating state compared with $T > T_N$, for which the liberated charges would give a spurious contribution to the polarization.

V. CONCLUSIONS

Structural, electrical polarization, and magnetodielectric characteristics of $LuCrO_3$ have been investigated. Similar studies carried out on $ErCrO_3$ enable us to compare the different orthochromites. The samples used for these investigations were found to be single phase with good crystallinity and quality from XRD and TEM investigations. The presence of twinning structure variants have been observed both in ECO and LCO samples by TEM studies. Polarization studies carried out after a poling process confirmed the existence of reversible remnant polarization just below T_N in both ECO and LCO. This unambiguously shows that the paramagnetic state of the R cation is not a necessary condition to observe such characteristics below T_N. Several hypotheses have been proposed to explain the observation of polarization, such as domain walls pinned by twin planes, a magnetostructural distortion below T_N responsible for Cr^{3+} off-centering, or a mechanism based on mixed valency leading to a spurious contribution. From the magnetodielectric studies, below the spin reorientation transition temperature T_{SR}, ECO exhibits a strong and positive MD(H) effect, which mimics the M(H) cycles supporting the existence of magnetoelastic coupling.

ACKNOWLEDGMENT

Author K.R.S.P acknowledges the MEET INTERREG project for supporting her postdoctoral fellowship.

[1] M. C. Weber, J. Kreisel, P. A. Thomas, M. Newton, K. Sardar, and R. I. Walton, Phys. Rev. B **85**, 054303 (2012).
[2] E. F. Bertaut, G. Bassi, G. Buisson, P. Burlet, J. Chappert, A. Delapalme, J. Mareschal, G. Roult, R. Aleonard, R. Pauthenet, and J. P. Rebouillat, J. Appl. Phys. **37**, 1038 (1966).
[3] E. F. Bertaut, J. Mareschal, G. de Vries, R. Aleonard, R. Pauthenet, J. P. Rebouillat, and V. Zarubicka, IEEE Trans. Magn. **2**, 453 (1966).
[4] K. P. Belov, A. K. Zvezdin, A. M. Kadomtseva, and R. Z. Levitin, Sov. Phys. Usp. **19**, 574 (1976).
[5] R. M. Honreich, S. Shtrikman, B. M. Wanklyn, and I. Yaeger, Phys. Rev. B **13**, 4046 (1976).
[6] D. Ullrich, R. Courths, and C. Von Grundherr, Physica B **89**, 205 (1977).
[7] F. Sayetat, J. Magn. Magn. Mater. **58**, 334 (1986).
[8] K. Toyokawa, S. Kurita, and K. Tsushima, Phys. Rev. B **19**, 274 (1979).
[9] A. Belik, Y. Matsushita, M. Tanaka, and E. Takayama-Muromachi, Chem. Mater. **24**, 2197 (2012).
[10] C. Moure, J. Tartaj, A. Moure, and O. Peña, J. Eur. Ceram. Soc. **32**, 3361 (2012).

[11] R. Courths, S. Hüfner, J. Pelzl, and L. G. Van Uetiert, Z. Physik **249**, 445 (1972).
[12] N. Shamir, H. Shaked, and S. Shtrikman, Phys. Rev. B **24**, 6642 (1981).
[13] B. Rajeswaran, D. I. Khomskii, A. K. Zvezdin, C. N. R. Rao, and A. Sundaresan, Phys. Rev. B **86**, 214409 (2012).
[14] T. Yamaguchi and K. Tsushima, Phys. Rev. B **8**, 5187 (1973).
[15] R. D. Johnson, N. Terada, and P. G. Radaelli, Phys. Rev. Lett. **108**, 219701 (2012).
[16] S. Geller and E. A. Wood, Act. Cryst **9**, 563 (1956).
[17] G. Van Tendeloo and S. Amelinckx, Acta Crystallogr. A **30**, 431 (1974).
[18] B. Lorenz, Y. Q. Wang, Y. Y. Sun, and C. W. Chu, Phys. Rev. B **70**, 212412 (2004).
[19] N. Bellido, C. Martin, Ch. Simon, and A. Maignan, J. Phys.: Condens. Matter **19**, 056001 (2007).
[20] J. D. Hurd, A. W. Simpson, and R. H. Tredgold, Proc. Phys. Soc. **73**, 448 (1959).
[21] L. G. Van Uitert, R. C. Sherwood, W. A. Bonner, W. H. Grodkiewicz, L. Pictroski, and G. Zydzik, Mater. Res. Bull. **5**, 153 (1970).
[22] E. M. Gyorgy and F. B. Hagedorn, J. Appl. Phys. **39**, 88 (1968).
[23] F. C. Rossol, Phys. Rev. Lett. **24**, 1021 (1970).
[24] A. P. Kuz'menko, J. Low Temp. Phys. **28**, 337 (2002).
[25] A. J. Kurtzig, IEEE Trans. Magn. **6**, 497 (1970).
[26] Y. Tokunaga, N. Furukawa, H. Sakai, Y. Taguchi, T. Arima, and Y. Tokura, Nat. Mater. **8**, 558 (2009).
[27] L. Oravova, Z. Zhang, N. Church, R. J. Harrison, C. J. Howard, and M. A. Carpenter, J. Phys.: Condens. Matter **25**, 116006 (2013).